Wireless Pers Commun (2010) 52:69–87
DOI 10.1007/s11277-008-9513-2

Impact of Mutual Coupling on Adaptive Switching Between MIMO Transmission Strategies and Antenna Configurations

Ramya Bhagavatula · Robert W. Heath Jr. · Antonio Forenza · Nicholas J. Kirsch · Kapil R. Dandekar

Published online: 28 May 2008

Abstract Adaptive switching between multiple-input multiple-output (MIMO) transmission strategies like diversity and spatial multiplexing is a flexible approach to respond to channel variations. It is desirable to obtain accurate estimates of the switching points between these transmission schemes to realize the capacity gains made possible by adaptive switching. In this paper, it is shown that the accuracy of switching point estimates for switching between statistical beamforming and spatial multiplexing is improved by taking into account the effects of mutual coupling between antenna array elements. The impact of mutual coupling on the ergodic capacities of these two transmission strategies is analyzed, by deriving expressions for the same. Adaptive switching between combinations of transmission strategies and antenna array configurations (using reconfigurable antenna arrays) is shown to produce maximum capacity gains. Expressions for the switching points between transmission strategies and/or antenna configurations, including mutual coupling effects, are derived and used to explore the influence of mutual coupling on the estimates. Finally, measurements taken from reconfigurable rectangular patch antenna arrays are used to validate the analytical results.

Keywords MIMO · Adaptive switching · Reconfigurable antenna arrays · Mutual coupling

R. Bhagavatula · R. W. Heath Jr. (✉)
The University of Texas at Austin, 1 University Station, C0803, Austin, Texas 78712-0240, USA
e-mail: rheath@ece.utexas.edu

R. Bhagavatula
e-mail: bhagavat@ece.utexas.edu

A. Forenza
Rearden, LLC, 355 Bryant Street, Suite 110, San Francisco, CA 94107, USA
e-mail: antonio@rearden.com

N. J. Kirsch · K. R. Dandekar
Drexel University, Philadelphia, 3141 Chestnut Street, Bossone 312, Philadelphia, PA 19104, USA
e-mail: njk27@drexel.edu

K. R. Dandekar
e-mail: dandekar@ece.drexel.edu

1 Introduction

Multiple-input multiple-output (MIMO) systems employ multiple antennas at the transmitter and receiver to introduce spatial degrees of freedom [1–3], which can be utilized to obtain higher link robustness using diversity schemes or higher capacity gains using spatial multiplexing. Beamforming is a diversity-based transmission strategy, where all the signal energy is sent across the strongest eigenmode of the channel [4,5]. Spatial multiplexing (SM) [6–8] is a transmission technique where a single data stream is split (or multiplexed) into multiple spatial streams, to provide high data rates with no sacrifice in bandwidth.

Adaptive switching between diversity schemes and spatial multiplexing can lead to higher link robustness and using limited feedback, can approach the capacity of a MIMO system with full channel knowledge at the transmitter [9–12]. Adaptive switching can occur using either instantaneous channel state information [10] or spatial correlation [11]. Using instantaneous channel state information for adaptive switching requires frequent feedback and may not be practical for rapidly varying wireless channels. In this paper, we use spatial correlation information for switching between transmission strategies. It has been shown in [13] that spatial correlation provides a good measure for the ergodic capacity and outage probability of a given system with multiple antennas at the transmitter. Hence, the spatial correlation of a channel plays a dominant role in determining the optimal transmit strategy. As it also varies more slowly than the instantaneous channel, adaptation using spatial correlation provides a balance between performance and reduced feedback requirements. Previous work on spatial correlation-based switching considered adaptive switching between diversity modes like statistical beamforming (SBF), and spatial multiplexing [11]. Switching points between these transmission strategies were derived, using ergodic capacity as a switching criterion in [11], as a function of the transmit and receive correlations in the channel, which in turn are a function of the channel and antenna parameters [14,15]. It has been shown in [15] that antenna geometry in particular has a significant impact on the achievable data rates.

In this article, we describe adaptive switching between combinations of antenna configurations and the transmission strategies, in response to varying channel conditions, to obtain maximum capacity gains [16,17]. The additional degree of freedom, obtained by varying antenna configurations, can be introduced using reconfigurable MIMO antenna arrays [18–22]. These antenna arrays, constructed using PIN diodes or RF MEMS switches, allow switching between different array configurations in response to changing channel statistics, to optimize performance criteria like bit error rate or capacity. Previous work in adaptive switching, however, does not take into account the impact of mutual coupling (MC) on the switching points between different transmission strategies and/or array configurations.

With the growing demand for smaller mobile handsets [23], multiple antennas can not be placed far apart. Consequently, the effect of mutual coupling (MC) on the achievable data rates can not be ignored. The impact of MC on channel capacity has been studied in [24–32]. In [24], it was shown that MC can increase system capacity, due to pattern diversity and in [25], the authors describe conditions beyond which MC will no longer affect the spatial correlation of the channel. The impact of MC on MIMO channel capacity has been studied in [26] from a network theory perspective, and in [27], by analyzing the combined influence of the channel matrix and SNR on systems performance. Expressions for the correlation matrix of a MIMO channel are derived in [28], in terms of MC. In [29], the authors use scattering matrices (called S-matrices) of the antenna systems to study MC effects. In [30] and [31], the authors propose methods to use MC to introduce pattern diversity and increase MIMO channel capacity. Finally, in [32], the impact of MC between the array elements on

the performance of the adaptive array antennas and on the design of adaptive algorithms is studied.

In our previous work [33], we analyzed the impact of antenna array configurations on the switching points between SBF and SM. We derived closed-form expressions for the switching points for a two element uniform linear array (ULA) as a function of antenna geometry and channel statistics. There has been no work done before to study the impact of MC on adaptive switching. In this paper, we study the impact of MC on switching between SBF and SM. The effect of MC on adaptive switching between combinations of transmission strategies and/or antenna array configurations (using reconfigurable antenna arrays) is also explored. We use measurement results taken using a reconfigurable rectangular patch antenna constructed in [17] to show that we can improve the accuracy of the switching points (in some instances, up to 15 dB improvement is seen), by including MC in the evaluation process. With adaptive switching fast gaining popularity due to its inclusion in standards like IEEE 802.16e [34], this improvement in accuracy is highly desirable. To summarize, in this paper, we

(1) derive ergodic capacity expressions for SBF and SM, including MC effects, and use them to show the impact of MC on the capacity gains obtained for SBF and SM,
(2) analyze adaptive switching between SBF and SM, by deriving switching point expressions, as a function of channel spatial correlation and the S-matrix of the antenna array configuration used,
(3) establish that adaptive switching between *both* the transmission strategy and/or array configuration (using reconfigurable antenna arrays) yields maximum capacity gains,
(4) derive expressions for switching between the transmission strategies and array configurations, as a function of the spatial correlation in the channel and antenna parameters (including MC effects), and
(5) use actual measurements taken from a reconfigurable rectangular patch antenna (used in [17]) to validate the analytical results.

The article is organized as follows. Section 2 describes the system and channel models, the antenna array configurations used, and the capacity evaluation, including MC. In Sect. 3, we derive ergodic capacity expressions for a MIMO channel using SBF and SM (for linear receivers), including MC. The switching points between SBF and SM are obtained in Sect. 3.3. We describe adaptive switching between transmission strategies and antenna array configurations, taking MC into account in Sect. 4. This is followed by the conclusion in Sect. 5.

2 System Description and Performance Evaluation

In this section, we describe the system and channel models, the antenna configuration and structure, and finally, capacity evaluation including mutual coupling effects.

2.1 System Model

Consider a MIMO system with M_T transmit and M_R receive antennas. Assuming a block time-invariant channel, the discrete-time input-output relation of the MIMO system (the discrete time index has been dropped for the sake of convenience) is given by

$$\mathbf{y} = \sqrt{\frac{E_s}{M_T}}\mathbf{H}\mathbf{s} + \mathbf{n} \tag{1}$$

where $\mathbf{y} \in \mathbb{C}^{M_R \times 1}$ is the received signal, $\mathbf{s} \in \mathbb{C}^{M_T \times 1}$ is the transmit signal constrained such that its covariance matrix, $\mathbf{R_{ss}} = \mathcal{E}\{\mathbf{ss}^\dagger\}$[1], satisfies $\mathrm{Tr}(\mathbf{R_{ss}}) = M_T$ and E_s is the total average energy available at the transmitter over a symbol period. The MIMO channel transfer matrix is denoted by $\mathbf{H} \in \mathbb{C}^{M_R \times M_T}$, and $\mathbf{n} \in \mathbb{C}^{M_R \times 1}$ is the complex additive white Gaussian noise at the receive antennas, with $\mathcal{E}\{\mathbf{nn}^\dagger\} = N_o \mathbf{I}_{M_R}$.

2.2 Channel Model

We use the popular Kronecker model [14,35] for our analysis of the narrowband MIMO system. According to the Kronecker model, the channel transfer matrix is given by

$$\mathbf{H} = \mathbf{R}_r^{1/2} \mathbf{H}_w \mathbf{R}_t^{1/2} \tag{2}$$

where $\mathbf{R}_t$ and $\mathbf{R}_r$ denote the transmit and receive spatial correlation matrices, respectively, and $\mathbf{H}_w \in \mathbb{C}^{M_R \times M_T}$, is a matrix of independent complex i.i.d. Gaussian entries with zero mean and unit variance. The channel matrix, $\mathbf{H}$, is normalized so that $\mathcal{E}\{\|\mathbf{H}\|_F^2\} = M_T M_R$. In the presence of a large amount of correlation, it has been shown in [36] that the capacity predicted by the Kronencker model is lower than the measured capacity and does not describe the multipath structure of the channel accurately [36–39]. In this article, however, we prefer to use the Kronecker model due to its analytical tractability. We use the clustered channel model [40] for our analysis. It is shown in [41] that channel models disregarding cluster effects overestimate channel capacity. The clustered model has also been validated through measurements [42,43] and variations have been used for different standards like IEEE 802.11n Technical Group [44] and the 3GPP Technical Specification Group [45] for system design and evaluation of cellular systems.

2.3 Antenna Design and Measurements

In this section, we discuss the antenna array architecture used in this paper and report on measured S-parameters. We do not describe the reconfigurable array configuration here, which is discussed in Sect. 4. We consider an array of two vertically polarized rectangular patch antennas. For our analysis, the performance of rectangular patch antennas operating at a frequency of 2.45 GHz was measured. The construction of the antenna array is shown in Fig. 1.

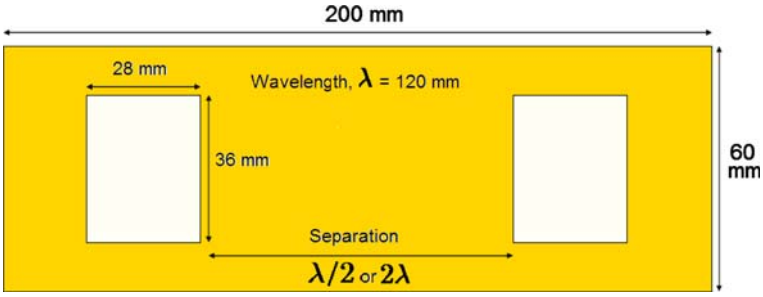

Fig. 1 Design and construction of the rectangular patch antenna array used in our analysis

[1] In this article, $\mathbf{X}$ refers to a matrix of the specified size. The transpose and Hermitian transpose of $\mathbf{X}$ is given by $\mathbf{X}^T$, and $\mathbf{X}^\dagger$ respectively. An identity matrix of size R is denoted by $\mathbf{I}_R$. Also, $\mathrm{Tr}(\mathbf{Y})$ and $|\mathbf{Y}|$ refer to the trace and determinant of a square matrix $\mathbf{Y}$, respectively. $\mathcal{E}\{.\}$ refers to the ergodic mean and $\|\mathbf{Y}\|_F$ stands for the Frobenius norm of $\mathbf{Y}$.

Table 1 Measured scattering parameters (magnitude in dB and angle in degrees) for the rectangular patch antenna arrays

Separation	S_{11}	S_{21}	S_{12}	S_{22}
$\lambda/2$	$-6.5\angle 33.6°$	$-21.4\angle 89.8°$	$-21.4\angle 89.8°$	$-8.0\angle -17.1°$
2λ	$-7.1\angle 29.7°$	$-25.3\angle 103.4°$	$-25.3\angle 103.4°$	$-6.4\angle 29.8°$

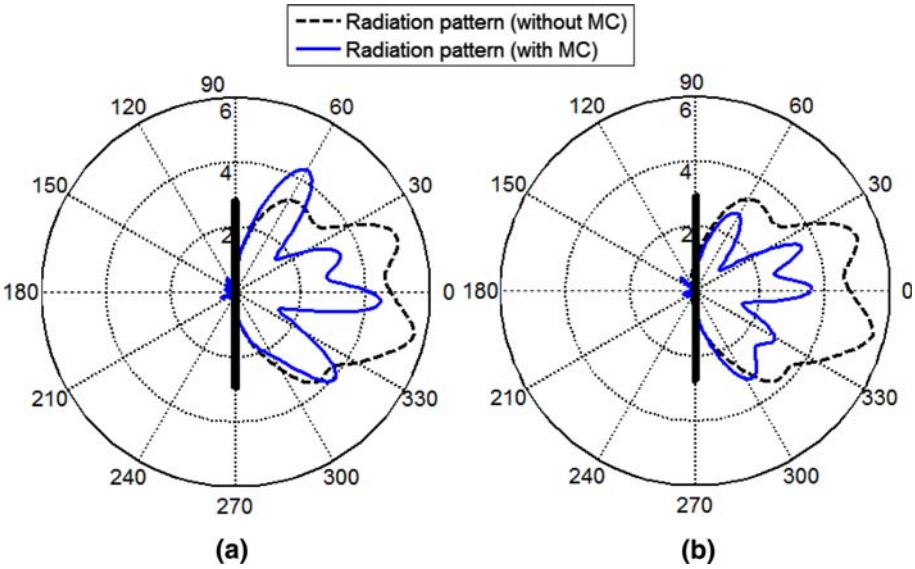

Fig. 2 Radiation patterns of the rectangular patch antennas, for an inter-element spacing (**a**) $\lambda/2$, and (**b**) 2λ. The radiation pattern of the antenna when we do not consider MC (given by the dashed line) has been superimposed for sake of comparison. The bold line in the center of the polar plots represent the plane of the rectangular patch antenna

The S-parameters were measured with a calibrated Agilent N5230A Network Analyzer by mounting the antennas at inter-element spacings of half wavelength and two wavelengths. The measured scattering parameter values corresponding to the antenna resonance frequency of 2.45 GHz for antenna element spacings of $\lambda/2$ and 2λ are given in Table 1, where λ refers to the wavelength. The radiation patterns associated with a rectangular patch antenna array, for inter-element spacings of $\lambda/2$ and 2λ are given in Fig. 2. The bold line in the middle of the polar plots in Fig. 2 represents the plane of the rectangular patch antennas. The radiation pattern of a single rectangular patch antenna (shown by a dashed line) has been superimposed on the plots, to make the pattern distortion caused by mutual coupling between the antenna elements evident. These antenna radiation patterns were obtained using FEKO [46], an electromagnetic software that relies on a hybrid method of moments and finite element method for simulating near-field propagation effects.

2.4 Capacity Performance

In this section, we describe an equivalent channel representation that takes into account mutual coupling, in terms of the S-matrices of the antenna arrays. The pattern distortion induced by mutual coupling is accounted for in the channel matrix, $\mathbf{H}$. Let the M_T and M_R

mutually coupled transmit and receive antennas be characterized by the S-matrices, $\mathbf{S}_T$ and $\mathbf{S}_R$ respectively. Then, from [47], the effective channel transfer matrix, $\mathbf{H}_{\text{eff}}$ is given by the two equivalent expressions in (3)

$$\begin{aligned} \mathbf{H}_{\text{eff}} &= (\mathbf{I}_{M_R} - \mathbf{S}_R)\, \mathbf{H} (\mathbf{I}_{M_T} - \mathbf{S}_T) \\ \mathbf{H}_{\text{eff}} &= (\mathbf{I}_{M_R} - \mathbf{S}_R) \mathbf{R}_r^{1/2}\, \mathbf{H}_w \mathbf{R}_t^{1/2} (\mathbf{I}_{M_T} - \mathbf{S}_T). \end{aligned} \tag{3}$$

We denote the transmit and receive coupling matrices by $\mathbf{C}_T = \mathbf{I}_{M_T} - \mathbf{S}_T$ and $\mathbf{C}_R = \mathbf{I}_{M_R} - \mathbf{S}_R$ respectively. When there is no mutual coupling on the transmit and receive antenna sides (when the antennas are placed far enough), then $\mathbf{C}_T = \mathbf{I}_{M_T}$ and $\mathbf{C}_R = \mathbf{I}_{M_R}$. This gives $\mathbf{H}_{\text{eff}} = \mathbf{R}_r^{1/2} \mathbf{H}_w \mathbf{R}_t^{1/2}$, as shown in (2). Hence, we see that (3) is a more general expression that reduces to the well known expression given by (2), in special cases.

We now show how the coupling matrices can be incorporated into the ergodic capacity expressions for a MIMO channel to account for MC effects. The ergodic capacity of a MIMO channel is given by

$$C = \max_{\mathbf{R}_{\text{ss}}} \mathcal{E} \left\{ \log_2 \left| \mathbf{I}_{M_R} + \frac{1}{N_o} \mathbf{H} \mathbf{R}_{\text{ss}} \mathbf{H}^{\dagger} \right| \right\} \frac{\text{b/s}}{\text{Hz}} \tag{4}$$

where the maximization is performed over all possible $\mathbf{R}_{\text{ss}}$, such that $\text{Tr}\,(\mathbf{R}_{\text{ss}}) = E_s$. To incorporate the effect of mutual coupling in (4), we replace $\mathbf{H}$ by $\mathbf{H}_{\text{eff}}$ to give

$$C = \max_{\mathbf{R}_{\text{ss}}} \mathcal{E} \left\{ \log_2 \left| \mathbf{I}_{M_R} + \frac{1}{N_o} \mathbf{H}_{\text{eff}} \mathbf{R}_{\text{ss}} \mathbf{H}_{\text{eff}}^{\dagger} \right| \right\} \frac{\text{b/s}}{\text{Hz}}. \tag{5}$$

We now show the impact of MC on the ergodic capacity of a MIMO channel. We consider the rectangular patch antenna array described in the previous section, with a spacing of

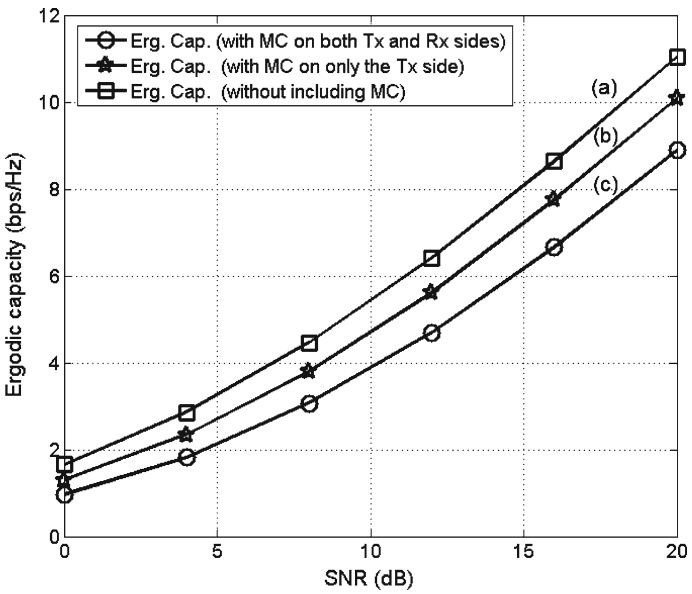

Fig. 3 Comparison of the ergodic capacities obtained for IEEE 802.11n channel model A, when (**a**) we do not consider mutual coupling at all, (**b**) we consider mutual coupling only on the transmit side, and (**c**) we consider mutual coupling at both the transmit and receive sides

$\lambda/2$ between the antenna elements. Using (5) and (4), the effect of MC is shown in Fig. 3, for the IEEE 802.11n channel model A [44]. It is seen from the figure that at SNR = 20 dB, the ergodic capacity obtained is overestimated by about 2.3 bps/Hz, when we do not consider the impact of mutual coupling at all. When we consider the impact of mutual coupling only at the transmit side, the ergodic capacity is lower by 1.3 bps/Hz, compared to the case when we do not consider mutual coupling at all. From this, it is evident that it is necessary to consider the impact of mutual coupling to get a realistic estimate of the actual capacity gains.

3 SBF and SM Capacity Analysis with MC

In this section, we derive expressions for the ergodic capacity of a MIMO system employing SBF and SM, incorporating MC effects. We analyze the impact of MC on the ergodic capacities of SBF and SM, using these expressions, for a single-sided correlated channel with zero correlation and zero mutual coupling between antenna elements at the receive side. From Fig. 3, it is evident that to get the maximum accuracy, we need to consider MC at both the transmit and receive sides. This, however, will make the derivations very complicated. Hence, to make our analysis tractable, we will consider only single-sided correlation at the transmit side and zero mutual coupling at the receiver, i.e. we let $\mathbf{S}_R = \mathbf{0}$ and $\mathbf{R}_r = \mathbf{I}_{M_R}$. We also assume that $M_T = M_R = M$ for simplicity.

3.1 Capacity of MIMO System Using SBF, Including MC

In this article, we analyze statistical beamforming [5], which is a low-complexity transmission strategy that sends all the data along the strongest eigenmode of the channel using statistical information of the channel at the transmitter, instead of instantaneous channel state information (to reduce feedback requirements).

Due to the assumption of single-sided correlation at the transmitter and zero MC at the receiver, we consider only the transmit side spatial correlation and S-matrices. Let the eigenvalue decomposition of the Hermitian transmit covariance matrix, $\mathbf{R}_t = \mathbf{U}_T \Lambda_T \mathbf{U}_T^{\dagger}$. Similarly, $\mathbf{C}_T = \mathbf{U}_{C_T} \Lambda_{C_T} \mathbf{U}_{C_T}^{\dagger}$. In SBF, since all the data is transmitted over the strongest channel, the transmit signal covariance matrix, $\mathbf{R}_{\mathbf{ss}}$ can be written as $\mathbf{R}_{\mathbf{ss}}^{BF} = \mathbf{U}_{R_{ss}}^{BF} \Lambda_{R_{ss}}^{BF} (\mathbf{U}_{R_{ss}}^{BF})^{\dagger}$, where $\Lambda_{R_{ss}}^{BF} = \text{diag}\{E_s, 0, 0, \ldots\}$. We associate the first column of $\mathbf{U}_{R_{ss}}^{BF}$ to correspond to the largest eigenvalue of the channel. Similarly, the first eigenvalues in the matrices Λ_{C_T} and Λ_T, correspond to the largest eigenvalues denoted by $\lambda_{C_T}^{\max}$ and $\lambda_T^{\max}$ respectively. For the case of single sided correlation at the transmit side and zero MC at the receive side, the ergodic capacity using SBF is obtained from (5) as

$$\begin{aligned} C_{\text{SBF}} &= \mathcal{E}\left\{\log_2\left|\mathbf{I}_M + \frac{1}{N_o}\mathbf{H}_{\text{eff}}\mathbf{R}_{\mathbf{ss}}\mathbf{H}_{\text{eff}}^{\dagger}\right|\right\} \\ &= \mathcal{E}\left\{\log_2\left|\mathbf{I}_M + \frac{1}{N_o}\mathbf{H}_w\mathbf{R}_t^{1/2}\mathbf{C}_T\mathbf{R}_{\mathbf{ss}}\mathbf{C}_T^{\dagger}\mathbf{R}_t^{\dagger/2}\mathbf{H}_w^{\dagger}\right|\right\} \end{aligned} \tag{6}$$

where (6) is obtained from (3) by letting $\mathbf{R}_r = \mathbf{I}_M$ and $\mathbf{C}_R = \mathbf{I}_M$. Simplifying (6) using the eigenvalue decompositions of $\mathbf{R}_t$, $\mathbf{C}_T$ and $\mathbf{R}_{\mathbf{ss}}$, and the matrix property $|\mathbf{I}_M + \mathbf{AB}| = |\mathbf{I}_M + \mathbf{BA}|$, we get

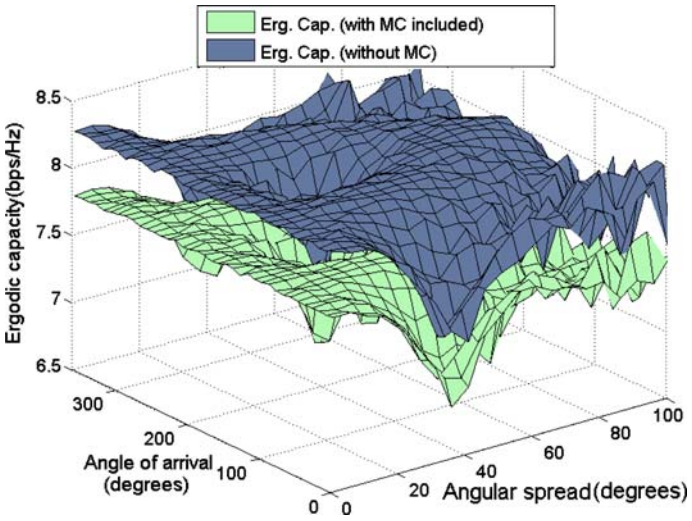

Fig. 4 Comparison of the ergodic capacities obtained for different angle of arrival and angular spread combinations, using statistical beamforming, for SNR = 20 dB

$$C_{\mathrm{SBF}} = \mathcal{E}\left\{\log_2\left|\mathbf{I}_M + \frac{E_s}{N_o}(\lambda_{C_T}^{\max})^2\lambda_T^{\max}\tilde{\mathbf{z}}\tilde{\mathbf{z}}^{\dagger}\right|\right\}$$
$$= \mathcal{E}\left\{\log_2(1+\rho(\lambda_{C_T}^{\max})^2\lambda_T^{\max}\tilde{\mathbf{z}}^{\dagger}\tilde{\mathbf{z}})\right\}\frac{\mathrm{b/s}}{\mathrm{Hz}} \tag{7}$$

where $\tilde{\mathbf{z}} = \left[z_1, z_2, \ldots, z_{M_R}\right]^T$. Here, z_i is a complex Gaussian random variable with zero mean and unit variance. Note that $\rho = E_s/N_o$. For the special case of zero mutual coupling at the transmit side, $\lambda_{C_T}^{\max} = 1$, reducing (7) to the expression in [11] (where mutual coupling between antenna elements was not taken into account)

$$C_{\mathrm{SBF}} = \mathcal{E}\left\{\log_2(1+\rho\lambda_T^{\max}\tilde{\mathbf{z}}^{\dagger}\tilde{\mathbf{z}})\right\}\frac{\mathrm{b/s}}{\mathrm{Hz}}.$$

An upper bound for the ergodic capacity of a MIMO system employing SBF can be obtained from (7) as

$$C_{\mathrm{SBF}} \leq \log_2(1+\rho\mathcal{E}\{(\lambda_{C_T}^{\max})^2\lambda_T^{\max}\mathcal{E}\{\tilde{\mathbf{z}}^{\dagger}\tilde{\mathbf{z}}\}\}) \tag{8}$$
$$= \log_2(1+\rho(\lambda_{C_T}^{\max})^2\lambda_T^{\max}\mathcal{E}\{\tilde{\mathbf{z}}^{\dagger}\tilde{\mathbf{z}}\}) \tag{9}$$
$$= \log_2(1+\rho(\lambda_{C_T}^{\max})^2\lambda_T^{\max}M_R)\frac{\mathrm{b/s}}{\mathrm{Hz}} \tag{10}$$

where (8) is obtained from Jensen's inequality, and (9), from the fact that $(\lambda_{C_T}^{\max})^2\lambda_T^{\max}$ is a constant. For the special case of no mutual coupling, (10) reduces to the upper bound obtained in [11].

We now proceed to show the impact of MC on the ergodic capacity of a MIMO system using SBF. Figure 4 compares the ergodic capacity of the case when MC is accounted for, to that obtained when MC is not included in the analysis, for different angles of arrival and angular spreads. The rectangular patch antenna array described in Sect. 2.3 is used with a spacing of $\lambda/2$, at SNR = 20 dB. We see that the difference in the two values of ergodic capacities can be as much as 2 bps/Hz. We further explore the impact of MC on the ergodic capacity

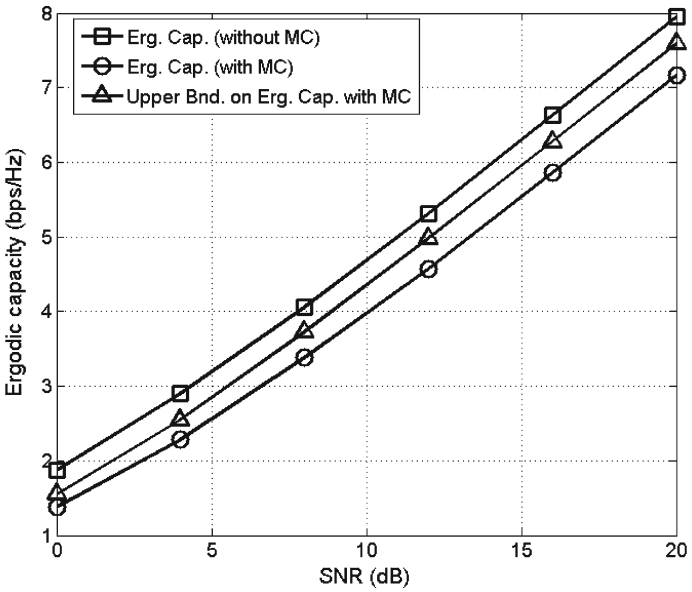

Fig. 5 Comparison of the ergodic capacities obtained for IEEE 802.11n channel model A, using statistical beamforming

obtained using SBF, and the closeness of the upper bound derived in (10) by using the IEEE 802.11n channel model A [44], for the same antenna array configuration. From Fig. 5, we see that that not considering the impact of MC will overestimate the ergodic capacity by about 1 bps/Hz over almost the entire SNR range, for this specific channel condition. The upper bound derived in (10) is also shown in Fig. 5. We can see that it is a very close approximation to the actual ergodic capacity curve. Also, for a spectral efficiency of 5 bps/Hz, we see that in practice, we need 3.5 dB (i.e. 2.24 times) more signal power, when we consider the impact of MC. Hence, it is evident that we need to account for MC effects to obtain more accurate estimates of the capacity gains.

3.2 Capacity of MIMO System Using Spatial Multiplexing, Including MC

For SM with linear receivers, the MIMO channel is decoupled into $M_T (= M)$ parallel streams [48]. Even though minimum mean-square error (MMSE) receivers outperform the zero-forcing (ZF) receivers, for the sake of simplicity, we consider only ZF receivers here. The conditional post-processing SNR for the kth stream for a ZF receiver, ρ_k, is given by

$$\rho_k = \frac{\rho}{M_T} \frac{1}{\left[(\mathbf{H}_{\text{eff}}^{\dagger} \mathbf{H}_{\text{eff}})^{-1} \right]_{k,k}} \tag{11}$$

where $\mathbf{H}_{\text{eff}}$ is given by (3) and $[\cdots]_{k,k}$ denotes the kth diagonal element. To make our analysis tractable, we make the assumption of single sided correlation at the transmit side and zero MC at the receive side, i.e. $(\mathbf{I}_{M_R} - \mathbf{S}_R)\mathbf{R}_r^{1/2} = \mathbf{I}_{M_R}$. We denote $\mathbf{R}_t^{1/2}(\mathbf{I}_{M_T} - \mathbf{S}_T) = (\widetilde{\mathbf{R}}_t)^{1/2}$. Then, from [11], the ergodic capacity of a MIMO system employing SM using a ZF receiver can be obtained as

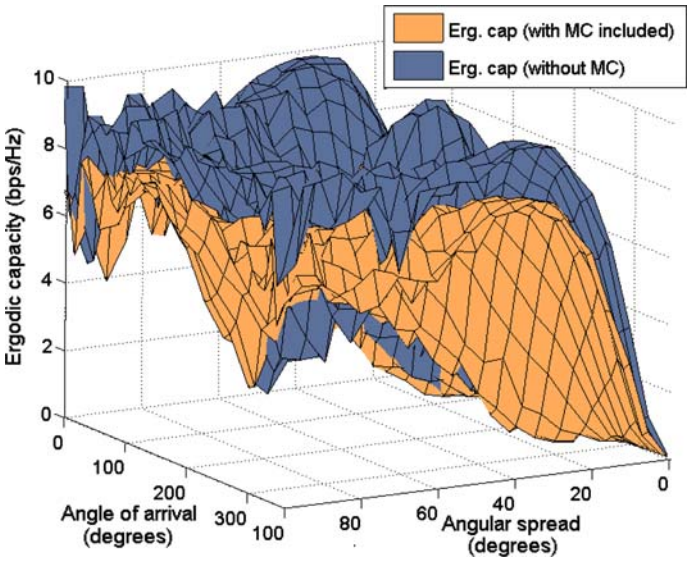

Fig. 6 Comparison of the ergodic capacities obtained for different angle of arrival and angular spread combinations, using spatial multiplexing, for SNR = 20 dB

$$C_{\mathrm{SM}} = \sum_{k=1}^{M} \frac{\mathrm{e}^{\left(\frac{|\widetilde{\mathbf{R}}_t^{kk}|M_T}{|\widetilde{\mathbf{R}}_t|\rho}\right)}}{\ln 2} \Gamma\left(0, \frac{|\widetilde{\mathbf{R}}_t^{kk}|M_T}{|\widetilde{\mathbf{R}}_t|\rho}\right) \tag{12}$$

where $\widetilde{\mathbf{R}}_t^{kk}$ corresponds to $\widetilde{\mathbf{R}}_t$ with the k^{th} row and column removed and $\Gamma(.,.)$ is the incomplete Gamma function.

An upper bound of the capacity of SM with ZF can be obtained from [11] to be

$$\begin{aligned} C_{\mathrm{SM}} &\leq \log_2\left(1 + \sum_{k=1}^{M} \rho^k \left(\frac{1}{M_T}|\widetilde{\mathbf{R}}_t|\right)^k \mathrm{tr}_k(\mathbf{A})\right) \\ &= \log_2\left(1 + \sum_{k=1}^{M} (\rho|\mathbf{C}_T|)^k \left(\frac{1}{M_T}|\mathbf{R}_t|\right)^k \mathrm{tr}_k(\mathbf{A})\right) \end{aligned} \tag{13}$$

where $\mathbf{A} = \mathrm{diag}(1/|\widetilde{\mathbf{R}}_t^{11}|, \ldots, 1/|\widetilde{\mathbf{R}}_t^{M_T M_T}|)$ and $\mathrm{tr}_k(.)$ denotes the kth elementary symmetric function (e.s.f.), defined as

$$\mathrm{tr}_k(\mathbf{X}) = \sum_{\underline{\alpha}} \prod_{i=1}^{k} \lambda_{x,\alpha_i} = \sum_{\underline{\alpha}} |\mathbf{X}_{\underline{\alpha}}^{\underline{\alpha}}| \tag{14}$$

for arbitrary Hermitian positive-definite $\mathbf{X} \in \mathbb{C}^{n\times n}$. In (14), the sum is over all ordered $\underline{\alpha} = \{\alpha_1, \ldots \alpha_k\} \subseteq \{1, \ldots, n\}$, $\lambda_{x,i}$ denotes the ith eigenvalue of $\mathbf{X}$, and $\mathbf{X}_{\underline{\alpha}}^{\underline{\alpha}}$ is the $k \times k$ principle submatrix of $\mathbf{X}$ formed by taking only the rows and columns indexed by $\underline{\alpha}$ [11].

Figure 6 compares the two cases when we include MC in our evaluation of the ergodic capacity of a MIMO system using SM and when we do not, for the rectangular patch antenna array described in Sect. 2.3 with a spacing of $\lambda/2$ at SNR = 20 dB. The difference in the two values of ergodic capacities is as much as 3.5 bps/Hz. This difference in ergodic capacities

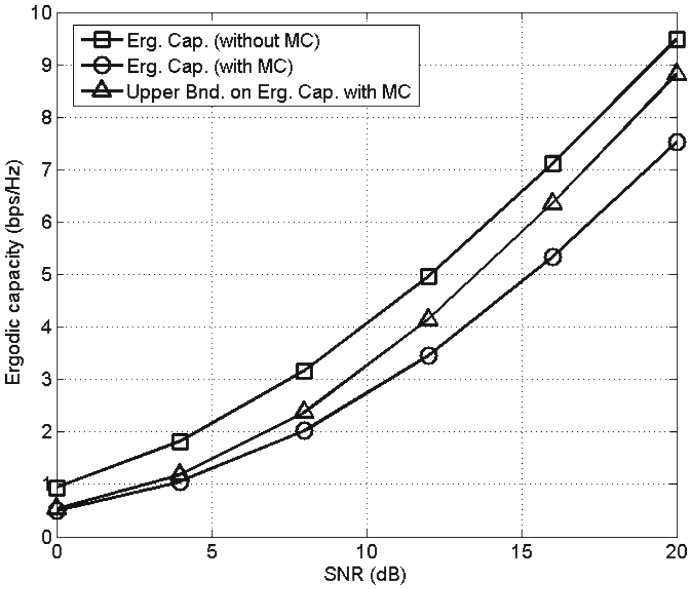

Fig. 7 Comparison of the ergodic capacities obtained for IEEE 802.11n channel model A, using spatial multiplexing

is much greater in the case of SM as compared to SBF. This is because calculation of the ergodic capacity for SM uses all the eigenvalues of the effective channel. In SBF, however, only the largest eigenvalue is used to calculate the ergodic capacity, as shown in (7). We further explore the impact of MC on the ergodic capacity of SM for the same configuration described above and for the IEEE 802.11n channel model A. It is seen from the figure that not considering the impact of MC will overestimate the ergodic capacity by 2 bps/Hz for SNR = 20 dB. The upper bound derived in (14) is also shown in Fig. 7. For a spectral efficiency of 5 bps/Hz, we see that in practice, we need 3.7 dB (i.e. 2.34 times) more signal power. Hence, accounting for MC is important to obtain realistic estimates of the capacity gains that can be obtained using SM.

3.3 Adaptive Switching between SBF and SM, Including MC

We use the ergodic capacity upper bounds from Sect. 3 to obtain closed-form expressions for the switching points between SBF and SM, including mutual coupling. As in the previous section, we consider single-sided correlation at the transmitter, zero MC at the receiver.

The switching point between SBF and SM is the positive root of the expression obtained by equating the upper bounds for both the cases, as given by equating (10) and (13), as per

$$\sum_{k=1}^{M} \rho_{\mathrm{CP}}^{k-1} \left(\frac{1}{M_T} |\widetilde{\mathbf{R}}_t| \right)^k \mathrm{tr}_k(\mathbf{A}) - (\lambda_{C_T}^{\max})^2 \lambda_T^{\max} M_R = 0 \,. \tag{15}$$

For $M_T = M_R = 2$, (15) can be simplified to

$$\rho_{\mathrm{CP}} = \frac{4(\lambda_{C_T}^{\max})^2 \lambda_T^{\max} - |\widetilde{\mathbf{R}}_t| \mathrm{tr}_1(\mathbf{A})}{\frac{1}{2}|\widetilde{\mathbf{R}}_t|^2 \mathrm{tr}_2(\mathbf{A})}. \tag{16}$$

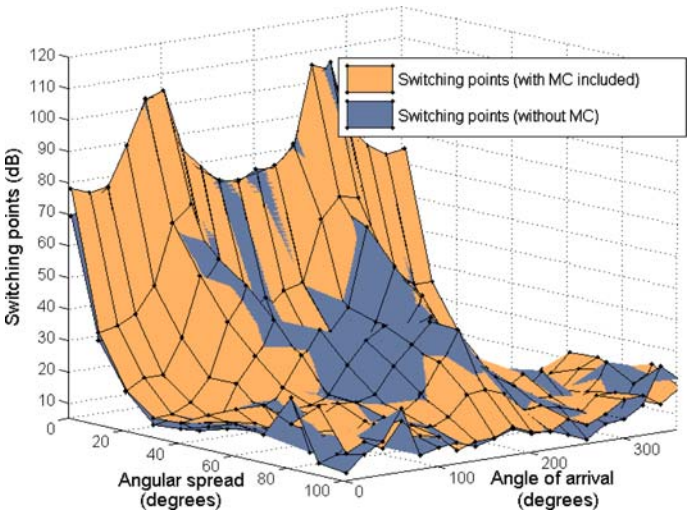

Fig. 8 Impact of mutual coupling on the switching points between SBF and SM for the rectangular patch array configuration with an inter-element spacing of $\lambda/2$

To illustrate our results, we consider the rectangular patch array with an inter-element spacing of $\lambda/2$ between the elements, as mentioned in the previous section. Figure 8 shows the variation of switching points (from (16)) over angles of arrival and angular spreads, when we take into account mutual coupling effects and when we do not, for SNR = 20 dB. Some of the switching points, particularly those for small angular spreads, are very high. This implies that for practical conditions, SBF will always be used, with the need for switching never arising, as SBF always outperforms SM for these low values of angular spreads. The difference in switching points as seen from the plot is as large as 14.5 dB for an angle of arrival (AoA) of 220° and an angular spread (AS) of 60°. A few other examples of the difference in switching point values include 6.28 dB for AS = 30° and AoA = 120°, 7.60 dB for AS = 30° and AoA = 160° and 5.58 dB for AS = 20°, AoA = 200°, etc. As Fig. 8 shows, we can obtain significantly more accurate estimates of the switching points between SBF and SM for a fixed configuration, if we consider the impact of mutual coupling.

4 Adaptive Switching between Transmission Schemes and Antenna Configurations

In this section, we show that adaptively switching between *both*—the transmission strategies and antenna configurations will lead to maximum capacity gains [17], in contrast to adaptively switching between only the transmission strategy for a fixed antenna configuration. We switch between combinations of transmission schemes and antenna array configurations, in response to varying channel conditions. For our analysis, we consider a reconfigurable MIMO array using the same rectangular patch antennas that we described in Sect. 2.3. We first describe the construction of the reconfigurable antenna array and then proceed to extend the switching point expressions obtained in Sect. 3.3 to the case where switching occurs between different transmission strategies and/or antenna configurations (including the effect of MC). We finally use the measurement results from Sect. 2.3, with the IEEE 802.11n channel model B [44] to verify our analysis.

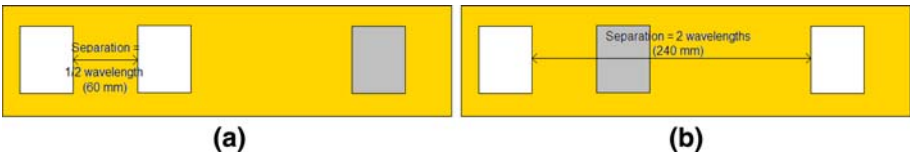

Fig. 9 Pictorial representation of the reconfigurable antenna arrays with three antenna elements, (**a**) represents an antenna array with element spacing $\lambda/2$, and (**b**) represents an antenna array with element spacing 2λ. It is to be noted that each circle represents each single antenna element

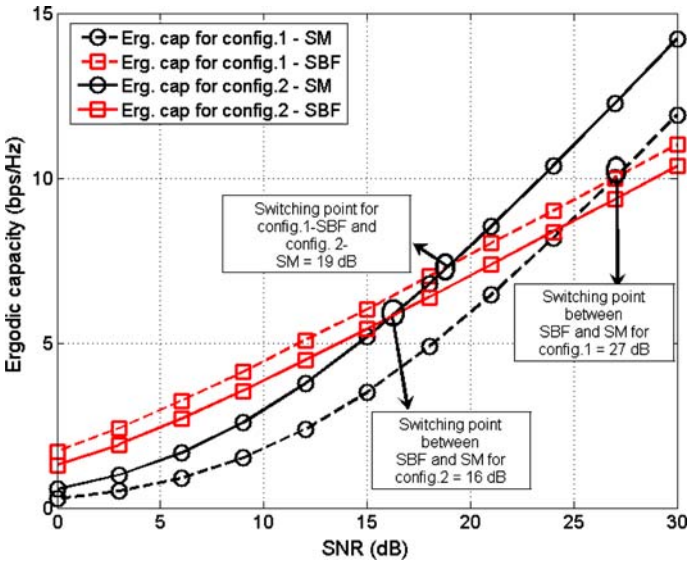

Fig. 10 Comparison of the switching points between configuration 1 and 2, and SBF and SM, to validate switching between transmission schemes and antenna array configurations

4.1 Reconfigurable Antenna Array Configuration

The reconfigurable antenna array is constructed using three rectangular patch antennas, as shown in Fig. 9. At any instant, only two of the three antennas (antennas 1 and 2 or antennas 1 and 3) are active, thereby yielding two different array configurations [17].

4.2 Switching Points between SBF and SM, for Different Configurations

The switching point expressions are derived from those in Sect. 3.3, by assuming that configuration 1 is used for SM and configuration 2 is used for SBF. In that case the switching point between configuration 1-SBF and configuration 2-SM, is obtained as

$$\rho_{\mathrm{CP}} = \frac{4(\lambda_{C_T,1}^{\max})^2 \lambda_{T,1}^{\max} - |\widetilde{\mathbf{R}}_{t,2}|\mathrm{tr}_1(\mathbf{A}_2)}{\frac{1}{2}|\widetilde{\mathbf{R}}_{t,2}|^2 \mathrm{tr}_2(\mathbf{A}_2)} \tag{17}$$

where $\lambda_{C_T,1}^{\max}$ and $\lambda_{T,1}^{\max}$ correspond to the maximum eigenvalues of the coupling matrix and the spatial correlation matrix at the transmit side respectively, for configuration 1, $\widetilde{\mathbf{R}}_{t,2}$ is the transmit correlation matrix for configuration 2, and $\mathbf{A}_2$ is defined for configuration 2.

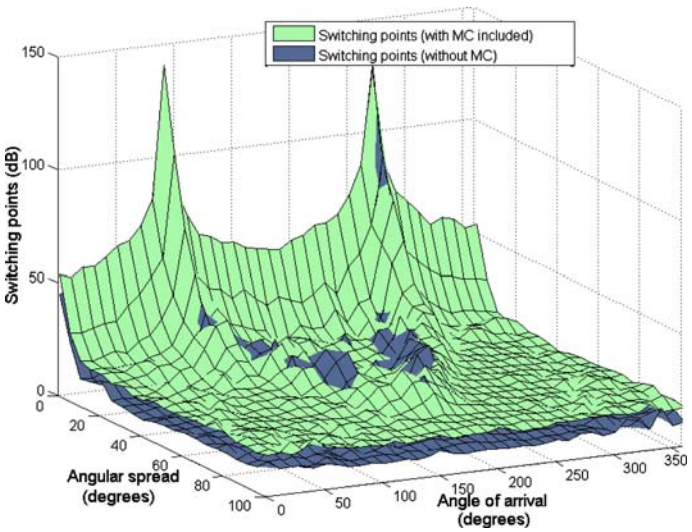

Fig. 11 Comparison of the switching points obtained for different angle of arrival and angular spread combinations, for configuration 1-SBF and configuration 2-SM at SNR = 20 dB

We motivate the need for adaptively switching between both the transmission strategy and configuration in Fig. 10. We employ the reconfigurable antenna described in Sect. 4.1, and use the IEEE 802.11n channel model B [44]. For sake of simplicity, we denote the array configuration in Fig. 9 with inter-element spacing $\lambda/2$ as configuration 1 and the configuration with inter-element spacing 2λ as configuration 2. From Fig. 10, we see that configuration 1 performs better for SBF and configuration 2 has higher ergodic capacity for SM. Thus, at 19 dB, if we switch from configuration 1-SBF to configuration 2-SM, we can obtain maximum capacity gains.

If we use a fixed antenna configuration 1, we would adaptively switch from SBF to SM only at SNR $\geq$27 dB, as shown in the figure. Thus, for all practical values of SNR, we would transmit using SBF. For SNR $\geq$ 19 dB, configuration 2-SM performs considerably better than configuration 1-SBF and configuration 1-SM, the difference in ergodic capacities being as large as 4 bps/Hz for SNR = 30 dB. Hence, by using only configuration 1, we lose the capacity gains that can be obtained by using configuration 2 for SNR $\geq$ 19 dB. On the other hand, if we use only configuration 2, we would lose 1 bps/Hz for all values of SNR $\leq$19 dB, as configuration 1-SBF outperforms configuration 2 in this SNR range. Thus, if we switch between configuration 1-SBF (that has the maximum ergodic capacity for SNR $\leq$ 19 dB) and configuration 2-SM (that has the maximum ergodic capacity for SNR $\geq$ 19 dB) at SNR = 19 dB, we obtain the best capacity gains.

We now proceed to show the impact of MC on the switching points when we switch adaptively between both the transmission schemes and the antenna array configurations. In Fig. 11, we plot the variation of switching point estimates, obtained from (17), between configuration 1-SBF and configuration 2-SM, for different AoAs and ASs at SNR = 20 dB. From Fig. 11, it is seen that we need to include MC in the evaluation of switching points to obtain significantly more accurate estimates. Examples of the large disparity in the switching point estimates, when we account for MC and when we do not, are 10.6 dB for AoA = 240° and AS = 16°, 10 dB for AoA = 50° and AS = 11°, 9.27 dB for AoA = 40° and AS = 40°,

etc. Thus, the benefits of adaptive switching can be realized by making the switching point estimates as accurate as possible, by incorporating MC effects.

This gives us an insight into how antenna geometries might be reconfigured adaptively in response to the channel parameters to improve performance. In particular, SBF benefits from using antennas that are close together as the higher correlation between the antenna elements allows the channel to have a stronger single spatial direction. SM works better with antennas that are further apart. This causes the multiple streams to have lower correlation between them, which is beneficial for SM. This motivates the development of reconfigurable MIMO antenna arrays.

5 Conclusion

In this article, we derived expressions for the ergodic capacities of two different MIMO transmission strategies, statistical beamforming and spatial multiplexing, by incorporating the effect of mutual coupling. We also derived expressions for the switching points between the two transmission strategies, taking into account mutual coupling effects, which can improve the accuracy of the estimated switching point by up to 15 dB. We also examined the effect of mutual coupling on the adaptive switching between antenna configurations and transmission strategies, to obtain maximum capacity gains. We conclude that accounting for mutual coupling effects when evaluating capacity gains, or switching points for adaptively switching between transmission strategies and/or antenna array configurations will improve the accuracy of the estimates significantly.

Acknowledgements The authors would like to thank Prathaban Mookiah, Drexel University, for his valuable contribution towards obtaining antenna measurements. This work is based in part upon work supported by Andrew Corporation.

References

1. Foschini, G. J., & Gans, M. J. (1998). On limits of wireless communications in a fading environment when using multiple antennas. *Wireless Personal Communication 6*(3), 311–335.
2. Paulraj, A. J., Gore, D. A., Nabar, R. U., & Bolcksei, H. (2004). An overview to MIMO communications—a key to Gigabit wireless. *Proceedings of the IEEE, 92*(2), 198–218.
3. Goldsmith, A., Jafar, S. A., Jindal, N., & Vishwanath, S. (2000). Capacity limits of MIMO channels. *IEEE Journal on Selected Areas in Communication, 48*(3), 502–513.
4. Jorswieck, E. A., & Boche, H. (2004). Channel capacity and capacity-range of beamforming in MIMO wireless systems under correlated fading with covariance feedback. *IEEE Transactions Wireless Communication, 3*, 1543–1553.
5. Kang, M., & Alouini, M. S. (2003). Water-filling capacity and beamforming performance of MIMO systems with covariance feedback. *IEEE Work on Signal Processing Advances in Wireless Communication*, 556–560.
6. Foschini, G. J. (1996). Layered space-time architecture for wireless communications in a fading environment when using multiple antennas. *Bell Laboratories Technical Journal, 1*(2), 41–59.
7. Golden, G. D., Foschini, G. J., Valenzuela, R. A., & Wolniansky, P. W. (1999). Detection algorithm and initial laboratory results using the V-BLAST space-time communications architecture. *IEEE Electronic Letters, 35*(7), 14–15.
8. Paulraj, A. J., & Kailath, T. (1994). Increasing capacity in wireless broadcast systems using distributed transmission/directional reception (DTDR). U. S. Patent 5,345,599, Sep. 1994.
9. Gesbert, D., Shafi, M., Shiu, D., Smith, P. J., & Naguib, A. (2003). From theory to practice: An overview of MIMO space time coded wireless systems. *IEEE Journal on Selected Areas in Communication, 21*(3), 281–302.

10. Heath, R. W., Jr., & Paulraj, A. J. (2005). Switching between diversity and multiplexing in MIMO systems. *IEEE Transactions on Communication, 53*(6), 962–968.
11. Forenza, A., McKay, M. R., Pandharipande, A., Heath, R. W., Jr., & Collings, I. B. (2005). Adaptive MIMO transmission for exploiting the capacity of spatially correlated channels. *IEEE Transactions on Vehicular Technology* (Accepted).
12. Catreux, S., Erceg, V., Gesbert, D., & Heath, R. W., Jr. (2002). Adaptive modulation and MIMO coding for broadband wireless data networks. *IEEE Communication Magazine, 40*(6), 108–115.
13. Jorswieck, E. A., & Boche, H. (2004). Optimal transmission strategies and impact of correlation in multiantenna systems with different types of channel state information. *IEEE Transactions on Signal Processing, 52*(12), 3440–3453.
14. Shiu, D. S., Foschini, G. J., Gans, M. J., & Kahn, J. M. (2000). Fading correlation and its effect on the capacity of multielement antenna systems. *IEEE Transactions on Communication, 48*(3), 502–513.
15. Forenza, A., & Heath, R. W., Jr. (2004). Impact of antenna geometry on MIMO communication in indoor clustered channels. *Proceedings of AP-S International Symposium, 2*, 1700–1703.
16. Piazza, D., & Dandekar, K. R. (2006). Reconfigurable antenna solution for MIMO-OFDM systems. *IEE Electronic Letters, 42* (8), 446–447.
17. Piazza, D., Kirsch, N. J., Forenza, A., Heath, R. W.,Jr., & Dandekar, K. R. (2007). Design and evaluation of a reconfigurable antenna array for MIMO systems. *IEEE Transactions on Antenna and Propagation* (Submitted Aug. 2006, revised Mar. 2007, accepted June).
18. Cetiner, B. A., Jafarkhani, H., Qian, J. Y., Yoo, H. J., Grau, A., & Flaviis, F. D. (2004). Multifunctional reconfigurable MEMS integrated antennas for adaptive MIMO Systems. *IEEE Communication Magazine, 42*, 62–70.
19. Anagnostou, D. E., Zheng, G., Chryssomallis, M. T., Lyke, J. C., Ponchak, G. E., Papapolymerou, J., & Christodoulou, C. G. (2006). Design, fabrication, and measurements of an RF-MEMS-based self-similar reconfigurable antenna. *IEEE Transactions on Antennal and Propagation, 54*, 422–432.
20. Jung, C. W., Lee, M. J., Li, G. P., & Flaviis, F. D. (2006). Reconfigurable scan-beam single-arm spiral antenna integrated with RF-MEMS switches. *IEEE Transactions on Antenna and Propagation, 54*, 455–463.
21. Huff, G. H., & Bernhard, J. T. (2006). Integration of packaged RF-MEMS switches with radiation pattern reconfigurable square spiral microstrip antennas. *IEEE Transactions on Antennas and Propagation, 54*, 464–469.
22. Yang, S. L. S., & Luk, K. M. (2006). Design of a wide-band l-probe patch antenna for pattern reconfiguration or diversity applications. *IEEE Transactions on Antennas and Propagation, 54*, 433–438.
23. Guo, Y. X., Chia, M. Y. W., & Chen, Z. N. (2004). Miniature built-in multiband antennas for mobile handsets. *IEEE Transactions on Antennas and Propagation, 52*(8), 1936–1944.
24. Svantesson, T., & Ranheim, A. (2001). Mutual coupling effects on the capacity of multielement antenna systems. *Proceedings of IEEE International Conference Acoustics, Speech, and Signal Processing, 2*, 2485–2488.
25. Li, X., & Nie, Z. P. (2004). Mutual coupling effect on the performance of MIMO wireless channels. *IEEE Antennas and Wireless Propagation Letters, 3*(1), 344–347.
26. Wallace, J. W., & Jensen, M. A. (2002). The capacity of MIMO wireless systems with mutual coupling. *Proceedings of the IEEE Vehicular Technoloygy Conference, 2*, 696–700.
27. Waldschmidt, C., Schulteis, S., & Wiesbeck, W. (2004). Complete RF system model for analysis of compact MIMO arrays. *IEEE Transactions on Vehicular Technology, 53*(3), 579–586.
28. Mbonjo, H. N. M., Hansen, J., & Hansen, V. (2004). MIMO Capacity and antenna array design. *IEEE Telecommunications Conference Proceedings Globecom, 5*, 3155–3159.
29. Wallace, J. W., & Jensen, M. A. (2004). Mutual coupling in MIMO wireless systems: A rigorous network theory analysis. *IEEE Transactions on Wireless Communication, 3*(4), 1317–1325.
30. Ohishi, T., Oodachi, N., Sekine, S., & Shoki, H. (2005). A method to improve the correlation coefficient and the mutual coupling for diversity antenna. *International Symposium on Antennas and Propagation Soceity, 1A*, 507–510.
31. Huang, Z., Balanis, C. A., & Birtcher, C. R. (2006). Mutual coupling compensation in UCAs: Simulations and experiment. *IEEE Transactions on Antennas and Propagation, 54*(11), 3082–3085.
32. Yuan, Q., Chen, Q., & Sawaya, K. (2006). Performance of adaptive array antenna with arbitrary geometry in the presence of mutual coupling. *IEEE Transactions on Antennas and Propagation, 54*(7), 1991–1996.
33. Bhagavatula, R., Forenza, A., & Heath, R. W., Jr. (2006). Impact of antenna array configurations on adaptive switching in MIMO channels. *Proceedings of International Symposium on Wireless Personal Multiple Communication*.
34. Erceg, V., et al. (2001). IEEE 802.16 broadband wireless access working Group. *IEEE 802.16.3c-01/29r4*, http://ieee802.org/16, Jul. 2001.

35. Kermoal, J. P., Schumacher, L., Pedersen, K. I., Mogensen, P. E., & Frederiksen, F. (2002). A stochastic MIMO radio channel model with experimental validation. *IEEE Journal on Selected Areas in Communication, 20*(6), 1211–1226.
36. Ozcelik, H., Herdin, M., Weichselberger, W., Wallace, J., & Bonek, E. (2003). Deficiencies of Kronecker MIMO radio channel model. *IEEE Electronic Letters, 39*(16), 1209–1210.
37. Weichselberger, W., Ozcelik, H., Herdin, M., & Bonek, E. (2003). A novel stochastic MIMO channel model and its physical interpretation. *International Symposium on Wireless Personal Multiple Communication*.
38. Wyne, S., Molisch, A. F., Almers, P., Eriksson, G., Karedal, J., & Tufvesson, F. (2005). Statistical evaluation of outdoor-to-indoor office MIMO measurements at 5.2 GHz. *Proceedings of IEEE Vehicular Technology Conference*, pp. 146–150.
39. Oestges, C., Ozcelik, H., & Bonek, E. (2005). On the practical use of analytical MIMO channel models. *Proceedings of IEEE Antennas and Propagation Symposium*, pp. 406–409.
40. Forenza, A., & Heath, R. W.,Jr. (2006). Benefit of pattern diversity via 2-element array of circular patch antennas in indoor clustered MIMO channels. *IEEE Transactions on Communication, 54* (5), 943–954.
41. Li, K., Ingram, M., & Van Nguyen, A. (2002). Impact of clustering in statistical indoor propagation models on link capacity. *IEEE Transactions on Communication, 50*(4), 521–523.
42. Saleh, A. M., & Valenzuela, R. A. (1987). A statistical model for indoor multipath propagation. *IEEE Journal Selected Areas in Communication, SAC-5*(2), 128–137.
43. Wallace, J. W., & Jensen, M. A. (2001). Statistical characteristics of measured MIMO wireless channel data and comparison to conventional models. *Proceedings of IEEE Vehicular Technology Conference, 2*(7–11), 1078–1082.
44. Erceg, V. et.al. (2004). TGn channel models. *IEEE 802.11-03/940r4*, http://www.802wirelessworld.com:8802/.
45. 3GPP Technical Specification Group. Spatial channel model, SCM-134 text V6.0. *Spatial Channel Model AHG (Combined as-hoc from 3GPP and 3GPP2)*.
46. Davidson, D. B., Theron, I. P., Jakobus, U., & Landstorfer, F. M. (1998). Recent progress on the antenna simulation program FEKO. *Proceedings of COMSIG Conference*, pp. 427–430.
47. Morris, M. L., & Jensen, M. A. (2005). Network Model for MIMO systems with coupled antennas and noisy amplifiers. *IEEE Transactions on Antennas and Propagation, 53*(1), 545–552.
48. Gore, D., Heath, R. W., Jr., & Paulraj, A. (2002). Transmit selection on spatial multiplexing systems. *IEEE Communication Letters, 6*, 491–493.

Author Biographies

Ramya Bhagavatula is a PhD student at The University of Texas at Austin. She received her BS degree in electrical and electronic engineering from Birla Institute of Technology and Sciences, Dubai, UAE in 2005, and the MS degree from The University of Texas at Austin in 2006. She won the 'IEEE Best student paper award' at the IEEE Vehicular Technology Conference, Spring 2007 in Dublin, Ireland. Her current research interests include analysis of MIMO antenna designs and MIMO channel modeling.

Robert W. Heath, Jr. received the B.S. and M.S. degrees from the University of Virginia, Charlottesville, VA, in 1996 and 1997 respectively, and the PhD from Stanford University, Stanford, CA, in 2002, all in Electrical Engineering. From 1998 to 2001, he was a Senior Member of the Technical Staff then a Senior Consultant at Iospan Wireless Inc., San Jose, CA where he worked on the design and implementation of the physical and link layers of the first commercial MIMO-OFDM communication system. In 2003 he founded MIMO Wireless Inc., a consulting company dedicated to the advancement of MIMO technology. Since January 2002, he has been with the Department of Electrical and Computer Engineering at The University of Texas at Austin where he is currently an Associate Professor and member of the Wireless Networking and Communications Group. His research interests cover a broad range of MIMO communication including limited feedback techniques, multihop networking, multiuser MIMO, antenna design, and scheduling algorithms as well as 60GHz communication techniques. Dr. Heath has been an Editor for the IEEE Transactions on Communication and an Associate Editor for the IEEE Transactions on Vehicular Technology. He is a member of the Signal Processing for Communications Technical Committee in the IEEE Signal Processing Society. He was a technical co-chair for the 2007 Fall Vehicular Technology Conference, is the general chair of the 2008 Communication Theory Workshop, and is a co-organizer of the 2009 Signal Processing for Wireless Communications Workshop. He is the recipient of the David and Doris Lybarger Endowed Faculty Fellowship in Engineering.

Antonio Forenza received the MS degree in telecommunications engineering from Politecnico di Torino, Italy, and Eurecom Institute, Sophia Antipolis, France, in 2001, and the PhD degree in electrical engineering from The University of Texas at Austin, TX, in 2006. In 2001, he interned as a Systems Engineer at Iospan Wireless, Inc., San Jose, CA, a startup company that developed the first commercial MIMO-OFDM communication system. His main research focus was on link-adaptation and physical layer algorithm design. In the fall 2001, he joined ArrayComm, Inc., San Jose, CA, as a Systems Engineer. In ArrayComm, he was actively involved in the design and implementation of smart antenna systems for the 3G WCDMA wireless platform. Over the summer 2004 and 2005, he interned as a Research Engineer at Samsung Advanced Institute of Technology (SAIT), Suwon, Korea, and Freescale Semiconductor, Inc., Austin, TX, respectively, developing adaptive MIMO transmission and MU-MIMO precoding techniques for 3GPP, IEEE 802.11n and IEEE 802.16e standards systems. Since June 2006, he has been working for Rearden, LLC, San Francisco, CA, as a Senior Systems Engineer. He authored the IEEE VTC'06 Best Student Paper Award and has published over 30 international journal and conference papers and standards contributions. His research interests include MIMO antenna design, adaptive MIMO transmission techniques, precoding methods for MU-MIMO, smart antenna signal processing.

Nicholas J. Kirsch received his BS degree in Electrical Engineering from the University of Wisconsin—Madison in 2003 with a focus on wireless communications. In 2006, he received a MS in Telecommunications Engineering from Drexel University in Philadelphia, PA. He worked at W. L. Gore & Associates in 2001–2002 on fiber optic link modules and long-wavelength lasers. Currently, he is a doctoral candidate in electrical and Computer Engineering at Drexel University. His research interests include MIMO communication systems, ad hoc networking, adaptive radio systems, and reconfigurable antennas.

Kapil R. Dandekar received the BS degree in Electrical Engineering from the University of Virginia in 1997 with specializations in communications and Signal Processing, Applied Electrophysics, and Computer Engineering. He received the MS and PhD degrees in Electrical and Computer Engineering from the University of Texas at Austin in 1998 and 2001, respectively. In 1992, he worked at the US Naval Observatory and from 1993–1997, he worked at the US Naval Research Laboratory. In 2001, Dandekar joined the Electrical and Computer Engineering Department as an Assistant Professor at Drexel University in Philadelphia, Pennsylvania. He is the Director of the Drexel Wireless Systems Laboratory (DWSL). DWSL has been supported by the US National Science Foundation, Army CERDEC, National Security Agency, Office of Naval Research, and private industry. Dandekars current research interests involve MIMO ad hoc networks, reconfigurable antennas, free space optical communications, ultrasonic communications, and sensor networks. He has published articles in several journals including IEEE Transactions on Antennas and Propagation, IEEE Transactions on Wireless Communications, IEEE Transactions on Communications, IEEE Transactions on Vehicular Technology, and IEE Electronics Letters. Dandekar currently serves on the editorial board of IEEE Expert Now and serves on the Pre-University Education Committee of the IEEE Educational Activities Board. He is a continuing active member of the Technical Program Committee for the IEEE Radio and Wireless Symposium. He serves as an Associate Editor for the IEEE Transactions on Vehicular Technology and is currently the chairman of the Philadelphia chapter of the IEEE Vehicular Technology.